

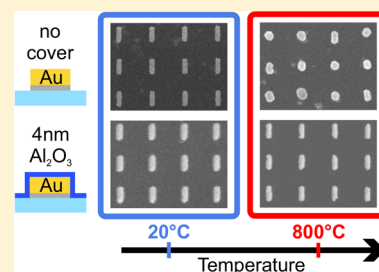
Refractory Plasmonics without Refractory Materials

Gelon Albrecht,^{*,†,‡,§} Stefan Kaiser,^{‡,†} Harald Giessen,[‡] and Mario Hentschel[‡][†]Max Planck Institute for Solid State Research, Heisenbergstraße 1, 70569 Stuttgart, Germany[‡]4th Physics Institute and Research Center SCoPE, University of Stuttgart, Pfaffenwaldring 57, 70569 Stuttgart, Germany

Supporting Information

ABSTRACT: Refractory plasmonics deals with metallic nanostructures that can withstand high temperatures and intense laser pulses. The common belief was that refractory materials such as TiN are necessary for this purpose. Here we show that refractory plasmonics is possible without refractory materials. We demonstrate that gold nanostructures which are overcoated with 4 and 40 nm Al₂O₃ (alumina) by an atomic layer deposition process or by thick IC1-200 resist can withstand temperatures of over 800 °C at ambient atmospheric conditions. Furthermore, the alumina-coated structures can withstand intense laser radiation of over 10 GW/cm² at ambient conditions without damage. Thus, it is possible to combine the excellent linear and nonlinear plasmonic properties of gold with material properties that were believed to be only possible with the lossier and less nonlinear refractory materials.

KEYWORDS: Plasmonic, refractory, thermal stability, gold nanostructures, THG, ambient atmosphere



Plasmons, the collective oscillations of free electrons in a plasma, have become a widely used phenomenon in current optical applications, for example in solar cells,¹ optical biomaterial sensing,² and for nonlinear optics.³ However, considering the vast range of applications, the utilized materials are still quite limited. Typically, either gold or silver are used, mainly due to their superior optical properties in the visible and infrared. Additionally, both materials exhibit a high optical nonlinear refractive index, rendering them excellent materials for nonlinear optics. Gold is furthermore chemically stable at ambient atmosphere, whereas silver quickly oxidizes.^{4,5} Regardless of their chemical stability, gold, as well as silver, are prone to thermally induced deformation. Already at an ambient temperature of 100 °C chemically grown gold nanoparticles start to deform,^{6–9} minimizing their surface energy.¹⁰ Within hours, the initially rod-like structures change into round structures. Intense laser exposure leads to heating and deformation of the structure.^{11–13} The structures become round during the heating process. For high fluences in the mJ/cm² range, structures fabricated on a substrate are immediately detached from the substrate and scattered throughout the sample.¹⁴ The deformation has direct impact on the plasmonic properties and will be visible in the optical spectrum of the nanoparticles. Most applications use the plasmonic resonance to absorb light or to detect changes in the refractive index around the plasmonic structure. All of these applications rely on stable optical properties of the plasmonic structure. Therefore, bare gold and silver are not suited for applications involving elevated temperatures or intense illumination.

To overcome this poor thermal stability, other materials were proposed to replace gold, namely the so-called refractory materials. A refractory material is defined by having a melting point beyond 2000 °C. For the near-infrared wavelength regime oxide materials such as indium–tin–oxide (ITO) were

demonstrated.^{15,16} Also nanostructured tungsten and molybdenum can be used in the infrared and withstand temperatures at least up to 900 °C in vacuum.^{17,18} Other materials with plasmonic properties in the infrared, however not refractory, are heavily doped GaAs and undoped InSb.^{16,19} Especially the transition metal nitrides such as titanium nitride (TiN) and zirconium nitride have been studied in great detail, exhibiting plasmon resonances even in the visible and near-infrared wavelength ranges.^{7,16,20–28} However, despite their excellent thermal properties, basically all known refractory materials exhibiting plasmonic properties are prone to oxidization and are chemically unstable, in particular when compared to gold. For example, titanium nitride has a melting point of 2977 °C,²⁹ yet it already oxidizes rapidly at 800 °C and loses its plasmonic properties.^{22,30} Consequently, these materials have to be kept under vacuum conditions²³ to prevent oxidization. Alternatively, the nanostructures can be buried in a protection layer,^{17,31} which was shown to work for some materials and applications. Many commonly used dielectrics, however, are oxides. It was shown, that oxygen from the oxide can diffuse into certain refractory materials, for example TiN, and cause oxidization.^{17,22}

Here, we demonstrate gold-based material systems for visible and near-infrared plasmonic applications to fabricate thermally and chemically stable nanostructures, without the limitations of, e.g., TiN or bare gold. To realize such systems, we applied the concept of a protection layer to gold nanostructures. Our protection layer is not supposed to prohibit chemical reactions, but rather to prevent the deformation of gold. We described in a previous publication³² that gold in a polymer matrix is more

Received: August 2, 2017

Revised: August 26, 2017

Published: August 30, 2017

stable upon laser exposure. The general idea of this concept has been widely used for many years.^{33–36} While these publications report first strong indications of the benefits of cover layers, no systematic study of the temperature nor of the thickness dependence have been performed. Both quantities are of fundamental as well as of practical importance. For example, thickly covered structures are not useful for plasmonic sensing type experiments. Thus, we significantly extend the previously reported results by studying the temperature evolution from room temperature up to 1100 °C, well above the gold melting temperature. We also show that already thin cover layers significantly stabilize the structures. What is more, we demonstrate the superior performance of the covered structures upon intense laser illumination, also highly important for various applications.

Besides the cover material, also the substrate material influences the stability of the nanostructures.^{37,38} Therefore, we compared Suprasil and Al₂O₃ as substrate materials. As cover material, we choose Al₂O₃ and IC1-200, a polysiloxane-based spin-on dielectric material, used for multilayer lithography. Al₂O₃ is a refractory material; however, it is a dielectric material and does not exhibit plasmon resonances. It is deposited by atomic layer deposition and forms an amorphous film (alumina). The Al₂O₃ substrate is commercially available sapphire glass. A summary of all material systems is shown in Figure 1. In all

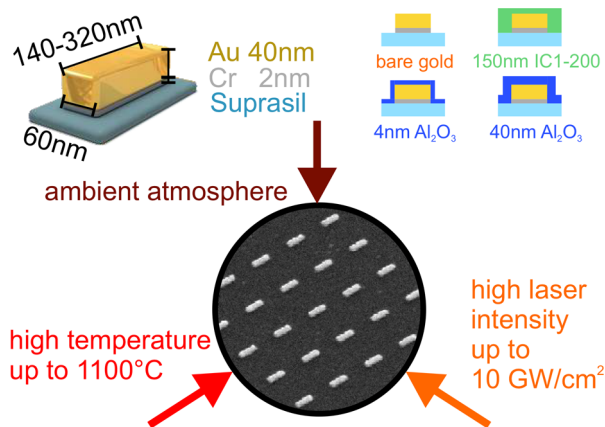


Figure 1. Geometrical parameters used for the rod nanostructures and the applied covers. In the bottom, visualization of degradation sources, which we applied to determine the damage threshold of our structures. The alumina-coated gold structures withstand heating up to 900 °C in ambient atmosphere, where bare gold rods or TiN rods are already destroyed. Furthermore, the alumina-covered gold rods show a stable optical third harmonic generation at 10 GW/cm² laser intensity, where bare gold rods already show strong degradation of the third harmonic signal.

further figures the pictographs introduced in this figure are used to indicate the corresponding material system. We have chosen the materials for two reasons: IC1-200 can be easily applied via spin-coating and is thus a cheap and straightforward way to coat even complex nanostructures. Atomic layer deposition of alumina is known to produce dense and crack-free films of well-controllable thickness. The material itself is expected to be extremely stable, while the defect-free layers also allow for ultimately thin, yet closed films. For such thin films of 4 nm thickness, the plasmonic near-field of the structure still significantly extends into the volume above the cover layer and thus allows for interaction with it for, e.g., sensing applications.

For the fabrication of the gold rod arrays, standard electron beam lithography is used. The metals are deposited on the Suprasil and sapphire substrates by thermal evaporation. The thicknesses are 2 nm chromium as the adhesion layer and 40 nm gold on top (see Figure 1). The chromium adhesion layer has a major effect on the stability of the gold structures³⁹ leading to an improved adhesion to the substrate and therefore increased dimensional stability. The width of the rods is chosen to be 60 nm. Their length is varied from 140 to 320 nm. All optical measurements are performed with light polarized parallel to the long rod axis. The lattice constant is 500 nm for both directions. The total area of one array is 80 μm × 80 μm. Scanning electron micrographs are shown in Figure 2. More SEM images are available in the Supporting Information. All structures are cleaned after the chemical lift-off by 20 s of oxygen plasma treatment. The IC1-200 coating is deposited by spin-coating (4000 rpm for 40s) and afterward annealed at 200 °C for 1 min. Finally, the film thickness was determined to be 150 nm for all of these samples by a stylus profiler. For the atomic layer deposition of Al₂O₃ (Cambridge NanoTech Savannah 100) trimethyl-aluminium (TMA) and water are used as precursor gases. The sample is heated to 250 °C during the process, resulting in a growth rate around 0.1 nm per cycle.

TiN nanostructures show strong oxidization at 800 °C, even in an argon-flushed environment.²² Therefore, as a first test for our proposed material systems, all covered and uncovered structures are exposed to 800 °C in ambient atmosphere to investigate the performance in comparison to TiN. The transmission spectra are measured with a commercial FTIR setup after preparation and after 1, 4, and 8 h exposed to 800 °C in air. The spectral data from a silicon detector and an InGaAs detector are stitched together, making it possible to measure the wavelength range from 600 to 1600 nm. First, the spectral evolution for the different material systems are compared for structures with a resonance around 1000 nm. Due to the different refractive indices of the surrounding, the length thus varies for different covers. The size dependence is discussed later and is depicted in Figure 5.

The optical transmission spectra for the bare gold rods are shown in the upper left panel of Figure 2. The upper right panels contain SEM micrographs of the rods before exposure to heat and after 8 h at 800 °C. The initially 220 nm long rods have strongly deformed to a circular shape, in agreement with literature.⁶ The deformation leads to a shrinking along the optically excited direction. This is reflected in the more than 300 nm shift of the center wavelength to lower wavelengths. Furthermore, the resonance is rather broad for gold at the respective wavelength. This can be attributed to the very inhomogeneous sizes of the deformed particles. Further SEM micrographs with a wider angle of view are provided in the Supporting Information.

In comparison, the rods coated with 4 nm alumina are still intact. The spectra show only a minor shift of the center wavelength toward shorter wavelengths and a small decrease in the full width at half-maximum (fwhm) of the resonance.

The third panel displays the 40 nm thick alumina-coated rods. The coating also protects the nanostructure from deformation. A small shift occurs, but toward longer wavelengths. A red shift could occur by an elongation of the nanostructures; however, this is unlikely. Alternatively the effective refractive index of the surrounding could change. This may occur due to a kind of sintering effect of the alumina. Another possibility is the formation of a thin gold-alumina intergranular film.⁴⁰ However, as the effect is not visible in case of a thin alumina coating, the

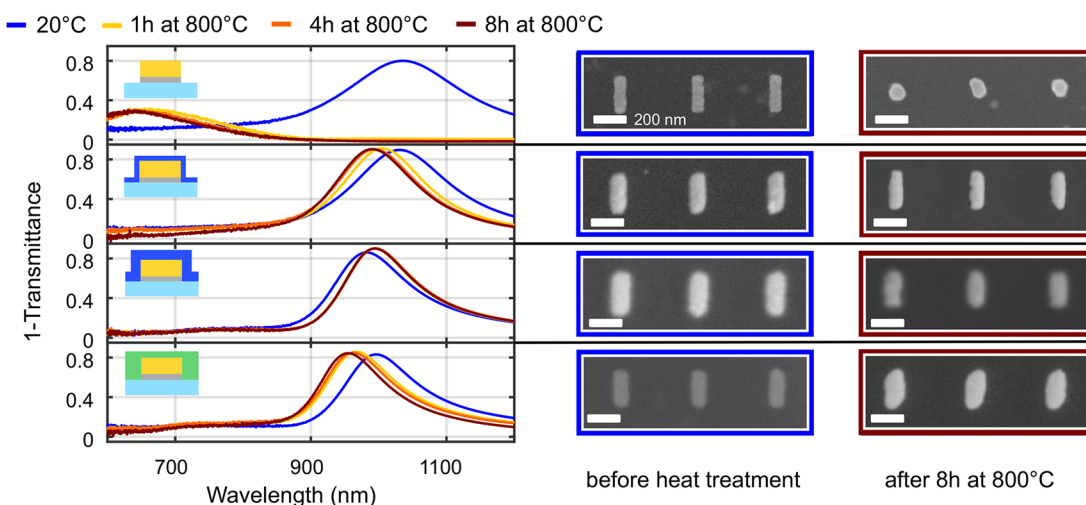


Figure 2. Left: Time-dependent change of the optical spectra for gold rods with different cover layers (from top: bare, 4 nm alumina, 40 nm alumina, 150 nm IC1-200), heated at 800 °C. Right: SEM images before and after heating; the scale bar is always 200 nm.

reason remains somewhat elusive at this point. It should be stressed, though, that the effect is minor and does by no means influence our interpretation. Another difference to the thin alumina coating the different measurements are barely discriminable, indicating that a steady state for the particle shape is reached faster.

Finally, the IC1-200-coated nanostructures show a slight shift of the resonance to shorter wavelengths. However, a small spectral shift is visible between all measurements. This behavior indicates that the IC1-200 system undergoes small changes for every time step and does not reach a steady state.

Besides the influence of the different covers, the influence of the chromium adhesion layer has to be emphasized. It is known to improve the thermal and dimensional stability of gold nanostructures. It has been shown that without chromium adhesion layer gold starts to already deform at temperatures of 100 °C.⁶ Thus, the chromium will in all cases contribute to the improved stability, in particular for the bare gold case. It has also been reported³⁹ that the chromium diffuses into the gold at elevated temperatures which is expected to partially degrade the plasmonic resonance. Our experiments, however, show a clear improvement of the plasmonic resonance with temperatures right up to the structural breakdown of the rod structures. It is thus very difficult to access the influence of chromium diffusion.

All three coatings significantly stabilize the gold resonance and keep the structures dimensionally stable. The alumina coating appears to be the most stable case. To check whether an all-alumina matrix would be even superior, the measurements are also conducted with a sapphire substrate. Intuitively, one would expect the geometry to be even superior with respect to its thermal stability. However, even though this material system prohibits the deformation, there is no major improvement compared to the Suprasil substrate. Application-wise, it is even counterproductive, as the strength of the initial resonance is substantially weaker. This is due to the higher refractive index of the substrate [$n_{\text{Suprasil}}(1000 \text{ nm}) = 1.45$; $n_{\text{sapphire}}(1000 \text{ nm}) = 1.75$]. Therefore, the rod length has to be smaller for the antenna to possess the same center wavelength. The smaller gold volume reduces the dipole strength and leads to a weaker resonance. The measurement is shown in the [Supporting Information](#).

To understand the thermal behavior of the different material systems, new samples of all four systems are fabricated and are

heated at increasing temperatures starting from 100 °C up to 1100 °C. After each step the transmission spectra are recorded. The samples are heated with two different heat sources. For temperature from 100 to 500 °C the samples are heated on a hot plate for 30 min in 50 °C steps. At higher temperatures ranging from 400 °C to 1100 °C, the samples are heated in a furnace for 60 min in 100 °C steps. The overlapping temperature range was measured to verify that the hot plate temperature was also reached at the position of the nanostructure. The spectra of the complete temperature cycle are displayed in [Figure 3a](#). For the

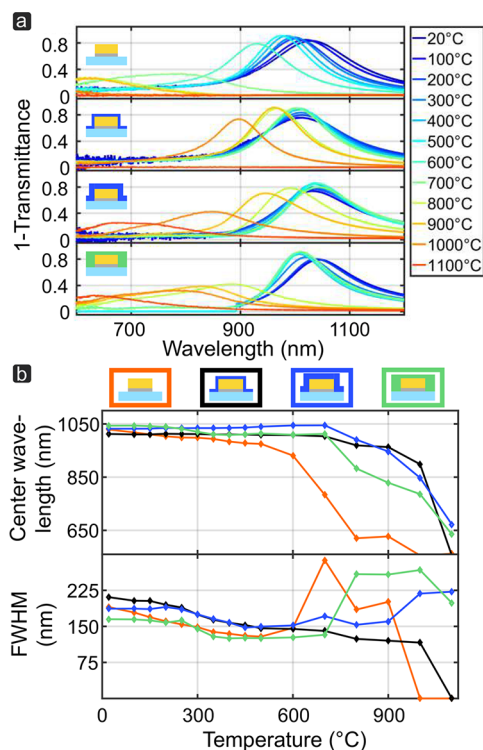


Figure 3. (a) Spectra for gold rods with different covers and without cover layer. The rods are subsequently heated at the indicated temperature for 30 min at 100 °C up to 500 °C on a hot plate and 60 min for the temperatures 600 °C up to 1100 °C in a furnace. (b) Extracted center wavelength and fwhm of the transmission spectra.

sake of clarity spectra are shown in 100 °C steps. In Figure 3b the center wavelength and the fwhm are extracted from the spectra. To do this for a strongly changing resonance in a rather robust way, the wavelength where the minimal transmission occurs is defined as the center wavelength. SEM images of the structures after the full temperature cycle are shown in Figure 4.

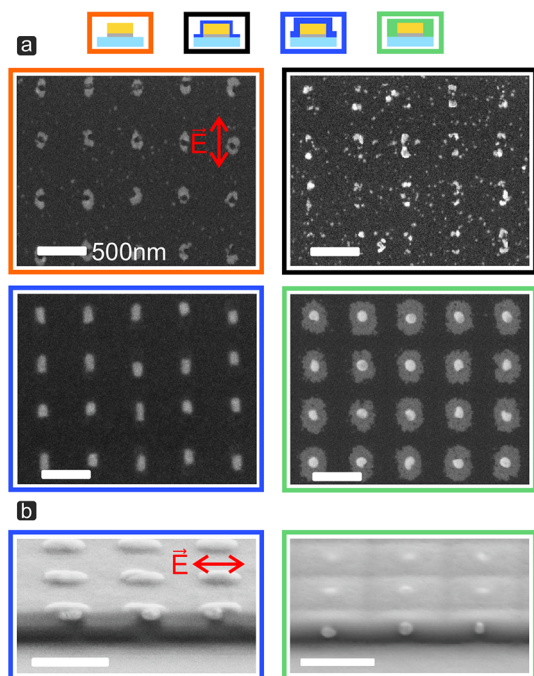


Figure 4. (a) SEM top down view after samples were heated up to 1100 °C. The measured polarization is indicated as a red arrow. (b) Cross-sectional SEM side view; the cross-section has been milled by focused ion beam; the scale bar is always 500 nm. The voids are visible as black features below the gold dots.

The top panel of Figure 3a shows the evolution of the transmittance spectrum of the bare gold rods. A uniform blue shift of the center wavelength, a decrease of the fwhm, and an increase of the resonance amplitude are visible up to 500 °C. After this temperature the center wavelength shifts rapidly to the blue; the fwhm increases, and the amplitude drops. At around 1000 °C, the resonance completely vanishes. For every temperature step, the spectra change, indicating a steady deformation of the nanostructure for each temperature step.

In the second panel the spectra of the 4 nm alumina-covered gold rods are depicted. The center wavelength of the structure remains unchanged until 700 °C; only the fwhm decreases, and the amplitude increases continuously. Even beyond 700 °C, the resonance shifts slightly up to 800 °C. What is more, it remains unchanged at the next temperature step to 900 °C. At 1000 °C the spectrum changes significantly and vanishes at 1100 °C.

The spectrum of the thick alumina-coated structure behaves qualitatively very similar to the thin cover up to 700 °C; the only difference is a small red shift of the center wavelength. This red shift is also visible for the sample heated constantly at 800 °C (see Figure 2). Above 700 °C the spectrum is continuously shifting to shorter wavelengths and starts to broaden above 900 °C. Even after 1100 °C a broad plasmon resonance is observed.

For the IC1-200-covered sample, a strong change in the spectra sets in at 700 °C. For temperatures from 350 to 700 °C, the center wavelength remains constant. At 350 °C a small shift

of the center wavelength is visible. This may be due to a shift of the refractive index of the IC1-200. The hard bake temperature of IC1-200 is 400 °C. However, it was only baked at 200 °C, which is sufficient for normal electron lithography usage.

Defining a thermal damage threshold based on the optical measurement is ambiguous. The easiest measure would be the center wavelength, which is directly related to the length of the resonantly excited rod.⁴¹ Nevertheless, in Figure 2, it is shown that despite a change in the center wavelength the shape of the structure remained nearly the same over hours. Also the fwhm is no ideal measure. For a single rod it would resemble the lifetime of the plasmon. The investigated structures are arrays of around 25 000 individual rods. Therefore, the fwhm reflects averaging effects as well. All four systems show a uniform decline of the fwhm in the beginning, which may be due to a sintering process. Sintering of metals can lead to a reduced resistance and a reduction of grain boundaries,^{36,42} which may result in a reduced fwhm. Beyond a certain temperature an increase in the fwhm is visible. This is most likely due to an increased length distribution of the rods, caused by the individual deformation process. For the bare gold and the IC1-200-coated sample the shift in center wavelength and the increase of the fwhm occur simultaneously, for the bare gold rods at 500 °C and the IC1-200-coated rods at 700 °C. However, the alumina-coated samples show a decreasing or constant fwhm up to 900 and 1000 °C, while their center wavelength is already shifted significantly. The shift may also be partly due to a change of the effective refractive index of the environment. This would imply that the cover layer changed, since changes in the bulk substrate are more unlikely. In combination with the long-term measurements at 800 °C, the alumina-coated structures are long-term stable after a short annealing time. Therefore, we estimate the damage threshold to be in the range from 800 to 1000 °C for these structures.

There are some distinct differences visible between the previous measurement at constant temperature of 800 °C (see Figure 2) and the measurement at 800 °C of this temperature series. The bare gold system and the thin alumina system look comparable. However, the thick alumina as well as the IC1-200 sample show a stronger degradation in the temperature series than in the measurement at constant temperature. This may be caused by the different thermal expansion properties of the different materials, which can lead to damages in the protective layer in every heating and cooling cycle. Furthermore, despite the similar fabrication conditions, the thermal stability will strongly depend on the interface properties among the coating, the gold structures, and the substrate. The adhesion of spin-coatable dielectrics to sample surfaces is known to critically depend on the exact surface conditions. Similarly, the formation of molecular layers during the ALD process is strongly dependent on the surface chemistry. While we tried to keep these properties as similar as possible by applying the plasma cleaning treatment, small differences are expected to already significantly influence the "sealing quality" of the overcoated and overgrown layers.

The coatings can stabilize the gold structures up to a temperature of at least 700 °C. This finding is supported by a report on carbon-coated gold nano rods, where structural deformations are visualized by transmission electron microscopy starting at around 700 °C.³³ The very similar temperature range for very different coatings suggests an effect independent of the coating material. For temperatures higher than 700 °C, degradation apparently starts to set in even for the covered structures. Especially the alumina coating prohibits a strong deformation up to around 900 °C and the two thick coatings

allow for the observation of a plasmon resonance up to a temperature of 1100 °C, which is above the melting point of bulk gold at 1064 °C.

After the complete temperature cycle up to 1100 °C, the samples are imaged with SEM. The micrographs are depicted in Figure 4. The upper four micrographs show a top-down view of the different samples. The bare gold and the thin alumina-coated samples show a complete destruction of the rods. Also 100 μm size marker structures completely vanished. Only strongly deformed structures can be observed; we suspect them to be parts of the chromium adhesion layer. We assume that the gold liquefied and completely diffused from the nanostructured area and accumulated in the surrounding, a process known as Oswald ripening.⁴³ However, in the close proximity of the nanostructured area, no accumulations of the gold are found. This finding is in accordance with the vanishing of the plasmon resonance in the transmittance spectrum.

The samples with the two thicker cover layers show a remaining plasmon resonance even after the complete temperature cycle. However, the resonance is extremely broad and quite far blue-shifted. Thus, on the basis of the optical measurements, it is expected that the gold structures have shrunk, and their size distribution is quite inhomogeneous. For both samples the rods can be clearly observed in the top-down SEM image and have changed their shape as expected. To obtain a side view of the structure, we applied focused ion beam (FIB) milling (Raith ionLINE Plus). The cover layer, as well as part of the structures, have been milled off to allow access to the side facet of the buried structures. Afterward, the sample is investigated by SEM (Figure 4b). For the alumina coating the cover layer is still intact, yet the gold particles have strongly deformed to a spherical shape inside the cover layer. Interestingly, it appears as if the alumina cover retained its shape and still shows the original extrusions of the rod like gold structure at the air interface. The gold particles seem to have detached from the substrate surface, leaving a dark void below them. However, it is mentioned that the influence of the FIB cut on the exact particle position is unclear. Furthermore, it is ambiguous where the exact alumina–Suprasil interface is located and therefore how strongly the particles have detached. It also appears for the IC1-200 cover that the structure has changed. The original cover film thickness was 150 nm. The film either has shrunk, or the particles have moved inside the cover layer, away from the substrate. The gold particles appear to have formed round particles, which would imply that they partly detached from the substrate. Further SEM images can be found in the Supporting Information.

To investigate the size dependence of the dimensional stability, the experiment that observes the temperature evolution at a constant temperature of 800 °C (Figure 2a), as well as the increasing temperature series are carried out with rods of varying lengths (Figure 5b). The rod length is varied in 20 nm steps from 140 to 320 nm. Only three of the lengths are presented here, because there is negligible difference between the different sizes. All sizes are shown in the Supporting Information. In Figure 5a, the extracted center wavelength and fwhm of the transmittance spectra for uncovered rods and rods covered with 4 nm alumina are depicted. The structures are exposed to a constant 800 °C. The bare gold rods exhibit a strong change of resonance wavelength as well as fwhm in the first time step. In the subsequent heating steps, no significant change is visible, in accordance with the previous results.

Furthermore, the aspect ratio from length to width plays an essential role for the strength of the change. The smaller the

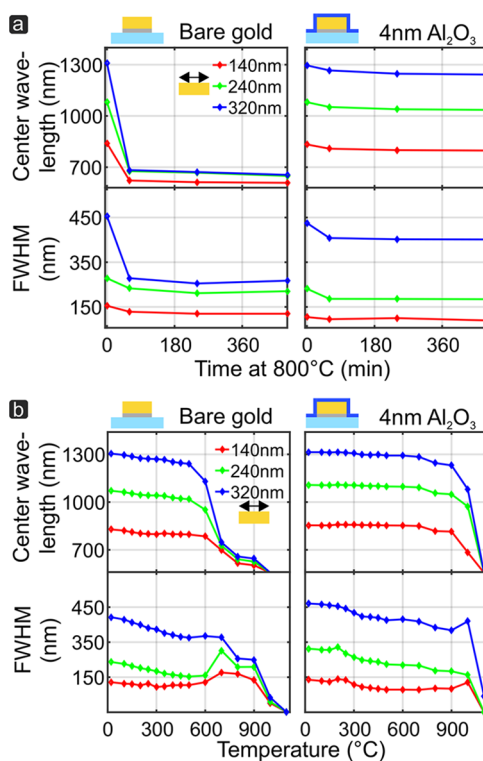


Figure 5. Change of the center wavelength and fwhm of the transmittance spectra of rods with different lengths. The left column depict bare gold rods and the right column shows rods with a 4 nm alumina cover exposed to 800 °C over a time of 480 min (a) and increasing temperatures (b). The samples in panel b are kept at the indicated temperature for 30 min for temperatures from 100 to 500 °C and 60 min for higher temperatures.

aspect ratio (the shorter the particle), the less the particle will shrink during the deformation to a circular shape. For the alumina-coated structures, a decrease in the center wavelength as well as in the fwhm is visible. Nevertheless, the change is far less pronounced, and the influence of the aspect ratio on the strength of change is visible. The size dependence of the temperature cycle presented in Figure 3 is depicted in Figure 5b. Also here all of the previously observed features are visible. The aspect ratio determines the strength of the change, but not the temperature stability. On the basis of these observations, a major size-dependent effect concerning the thermal stability of the gold rods can be excluded. The data for the two thick covers are in excellent agreement with this conclusion and can be found in the Supporting Information.

Intense laser illumination at high repetition rates and low pulse energies generates heat and strong local electric fields in plasmonic nanostructures, causing significant damage to the investigated nanostructures. Having our findings in mind, we expect that the increased stability of our covered nanostructures should also lead to an increased damage threshold for laser illumination. To test this assumption, the material systems are exposed to 10 GW/cm² of laser radiation, well above the fluence normally used for nonlinear spectroscopy.⁴⁴ As a measure of the stability, the temporal evolution of the generated third harmonic (TH) intensity is studied. Apart from the fact that many applications of nonlinear plasmonics in fact use TH generation, we also choose this measure as the signal is known to crucially depend on the exact shape of the plasmonic resonance.⁴⁵ The measurement is performed with an in-house build laser source

(Figure 6a).^{21,46} The laser source provides a spectrum ranging from 950 to 1150 nm with a pulse duration of 16 fs, a repetition

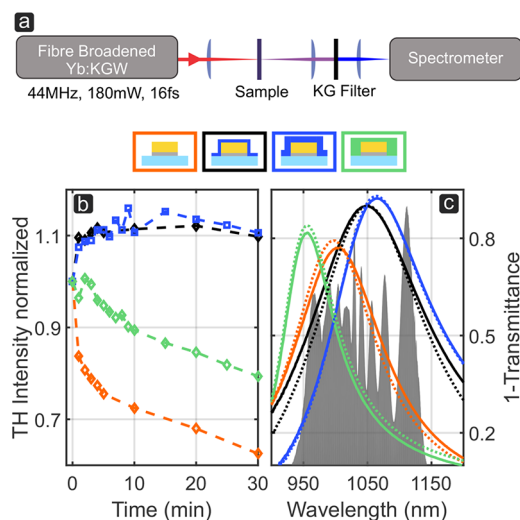


Figure 6. (a) Experimental setup for the third harmonic spectroscopy; (b) TH intensity of covered and bare gold rods exposed to 10 GW/cm² laser radiation (180 mW, beam fwhm 32 μ m). (c) Transmittance spectra of the nanostructure types before (solid line) and after 30 min laser exposure (dashed line); the laser spectrum is displayed in gray.

rate of 44 MHz, and a maximum average power of 180 mW before the focusing lens in front of the sample. To remove all spectral components below 700 nm, a 3 mm thick Schott RG715 filter is placed before the sample. The beam at the focal point has a fwhm of 32 μ m, measured by a knife edge test. The TH is detected with a Peltier-cooled charge-coupled device, after the fundamental beam is strongly attenuated (Schott glasses, 6 mm KG5 and 3 mm KG4). The measured TH intensity is shown in Figure 6b. The TH response is normalized for all structures to the TH of the respective structure at time zero. For both alumina-coated rods a substantial increase of the TH in the first time step is visible. Afterward the TH intensity remains constant for the rest of the measurement. The linear spectrum should reflect this change. For both alumina-coated samples, a rather small decrease of the fwhm is visible. However, in the anharmonic oscillator model for nonlinear plasmonic processes the fwhm enters at the sixth power,³ indicating that already small changes in the fwhm, i.e., the quality factor of the resonance, lead to significant changes in the signal strength. Similar results have been reported recently.²¹

The TH of the bare gold structure and the IC1-200-covered structure continuously decrease. The reason is the change of the linear spectra, which changes and shifts to shorter wavelengths out of the overlap with the laser spectrum, resulting in a reduced nonlinear signal. We have shown that the alumina overcoated structures exhibit a significantly increased damage threshold compared to the bare structures, but also when compared to the IC1-200-coated structures. The changes of the signal strength (i.e., the increased TH) is related to the change in the quality factor which most likely stems from a local heating of the sample, very similar to the increase in quality factor observed in the heating experiments discussed above.

In summary, we presented three different gold based plasmonic systems, which combine the thermal stability of a refractory material and the chemical stability of gold. The alumina coating nearly doubles the thermal damage threshold

compared to the bare gold and outperforms titanium nitride systems. The exact thermal damage threshold varies slightly from sample to sample, yet it is significantly enhanced from 500 $^{\circ}$ C to around 900 $^{\circ}$ C. What is more, we demonstrate the superior damage threshold for intense laser illumination at least up to 10 GW/cm². The thickness of the protection layer can be as thin as 4 nm, without losing its protective properties. This thickness is thin enough to still access the enhanced near field of the plasmonic structure. Therefore, the cover does not hamper the usage of the system in refractive index sensing applications. All in all, our concept extends the scope for gold nanostructures to high temperature, ambient atmosphere, and intense illumination applications, overcoming the chemical stability limitations of refractory materials and the thermal stability limitations of bare gold.

■ ASSOCIATED CONTENT

Supporting Information

The Supporting Information is available free of charge on the ACS Publications website at DOI: 10.1021/acs.nanolett.7b03303.

Transmission spectra of an all-alumina system; wide angle SEM images of the different material systems after 8 h at 800 $^{\circ}$ C and after the full temperature cycle up to 1100 $^{\circ}$ C; temperature dependence of the resonance for varying rod lengths (PDF)

■ AUTHOR INFORMATION

Corresponding Author

*E-mail: g.albrecht@pi4.uni-stuttgart.de.

ORCID

Gelon Albrecht: 0000-0002-5456-2864

Notes

The authors declare no competing financial interest.

■ ACKNOWLEDGMENTS

We acknowledge support from ERC (Complexplas), BMBF, DFG (SPP 1839), MWK BW under the Juniorprofessorenprogramm, Daimler und Benz Stiftung, and BW Stiftung. G A acknowledges funding from Max Planck Institute for Solid State Research. We thank Marion Hagel for fabricating the ALD layers. Also we would like to thank Shahin Bagheri and Rotraut Merkle for fruitful discussions about refractory materials.

■ REFERENCES

- (1) Catchpole, K.; Polman, A. *Opt. Express* **2008**, *16*, 21793–21800.
- (2) Schultz, D. A. *Curr. Opin. Biotechnol.* **2003**, *14*, 13–22.
- (3) Hentschel, M.; Utikal, T.; Giessen, H.; Lippitz, M. *Nano Lett.* **2012**, *12*, 3778–3782.
- (4) Yin, Y.; Li, Z.-Y.; Zhong, Z.; Gates, B.; Xia, Y.; Venkateswaran, S. *J. Mater. Chem.* **2002**, *12*, 522–527.
- (5) Thyagarajan, K.; Santschi, C.; Langlet, P.; Martin, O. J. *Adv. Opt. Mater.* **2016**, *4*, 871–876.
- (6) Petrova, H.; Perez Juste, J.; Pastoriza-Santos, I.; Hartland, G. V.; Liz-Marzán, L. M.; Mulvaney, P. *Phys. Chem. Chem. Phys.* **2006**, *8*, 814–821.
- (7) Liu, Y.; Mills, E. N.; Composto, R. J. *J. Mater. Chem.* **2009**, *19*, 2704–2709.
- (8) Mohamed, M. B.; Ismail, K. Z.; Link, S.; El-Sayed, M. A. *J. Phys. Chem. B* **1998**, *102*, 9370–9374.
- (9) Gou, L.; Murphy, C. J. *Chem. Mater.* **2005**, *17*, 3668–3672.
- (10) Wang, Y.; Teitel, S.; Dellago, C. *Nano Lett.* **2005**, *5*, 2174–2178.

- (11) Link, S.; Burda, C.; Nikoobakht, B.; El-Sayed, M. A. *J. Phys. Chem. B* **2000**, *104*, 6152–6163.
- (12) Kuhlicke, A.; Schietinger, S.; Matyssek, C.; Busch, K.; Benson, O. *Nano Lett.* **2013**, *13*, 2041–2046.
- (13) Inasawa, S.; Sugiyama, M.; Yamaguchi, Y. *J. Phys. Chem. B* **2005**, *109*, 3104–3111.
- (14) Gentile, M.; Hentschel, M.; Taubert, R.; Guo, H.; Giessen, H.; Fiebig, M. *Appl. Phys. B: Lasers Opt.* **2011**, *105*, 149–162.
- (15) Naik, G. V.; Kim, J.; Boltasseva, A. *Opt. Mater. Express* **2011**, *1*, 1090–1099.
- (16) Naik, G. V.; Shalaev, V. M.; Boltasseva, A. *Adv. Mater.* **2013**, *25*, 3264–3294.
- (17) Park, J. H.; Han, S. E.; Nagpal, P.; Norris, D. *ACS Photonics* **2016**, *3*, 494–500.
- (18) Arpin, K. A.; Losego, M. D.; Cloud, A. N.; Ning, H.; Mallek, J.; Sergeant, N. P.; Zhu, L.; Yu, Z.; Kalanyan, B.; Parsons, G. N.; Girolami, G. S.; Abelson, J. R.; Fan, S.; Braun, P. V. *Nat. Commun.* **2013**, *4*, 2630.
- (19) Hanham, S.; Fernández-Domínguez, A.; Teng, J. H.; Ang, S.; Lim, K.; Yoon, S. F.; Ngo, C.; Klein, N.; Pendry, J.; Maier, S. A. *Adv. Mater.* **2012**, *24*, OP226.
- (20) Guler, U.; Boltasseva, A.; Shalaev, V. M. *Science* **2014**, *344*, 263–264.
- (21) Gui, L.; Bagheri, S.; Strohfeldt, N.; Hentschel, M.; Zgrabik, C. M.; Metzger, B.; Linnenbank, H.; Hu, E. L.; Giessen, H. *Nano Lett.* **2016**, *16*, 5708–5713.
- (22) Bagheri, S.; Zgrabik, C. M.; Gissibl, T.; Tittl, A.; Sterl, F.; Walter, R.; De Zuan, S.; Berrier, A.; Stauden, T.; Richter, G.; Hu, E. L.; Giessen, H. *Opt. Mater. Express* **2015**, *5*, 2625–2633.
- (23) Wang, Y.; Capretti, A.; Dal Negro, L. *Opt. Mater. Express* **2015**, *5*, 2415–2430.
- (24) Briggs, J. A.; Naik, G. V.; Petach, T. A.; Baum, B. K.; Goldhaber-Gordon, D.; Dionne, J. A. *Appl. Phys. Lett.* **2016**, *108*, 051110.
- (25) Li, W.; Guler, U.; Kinsey, N.; Naik, G. V.; Boltasseva, A.; Guan, J.; Shalaev, V. M.; Kildishev, A. V. *Adv. Mater.* **2014**, *26*, 7921–7921.
- (26) Guler, U.; Ndukaiife, J. C.; Naik, G. V.; Nnanna, A. A.; Kildishev, A. V.; Shalaev, V. M.; Boltasseva, A. *Nano Lett.* **2013**, *13*, 6078–6083.
- (27) Naik, G. V.; Schroeder, J. L.; Ni, X.; Kildishev, A. V.; Sands, T. D.; Boltasseva, A. *Opt. Mater. Express* **2012**, *2*, 478–489.
- (28) Zgrabik, C. M.; Hu, E. L. *Opt. Mater. Express* **2015**, *5*, 2786–2797.
- (29) Molesky, S.; Dewalt, C. J.; Jacob, Z. *Opt. Express* **2013**, *21*, A96–A110.
- (30) Mitsuo, A.; Uchida, S.; Nihira, N.; Iwaki, M. *Surf. Coat. Technol.* **1998**, *103*, 98–103.
- (31) Liu, J.; Guler, U.; Lagutchev, A.; Kildishev, A.; Malis, O.; Boltasseva, A.; Shalaev, V. M. *Opt. Mater. Express* **2015**, *5*, 2721–2728.
- (32) Albrecht, G.; Hentschel, M.; Kaiser, S.; Giessen, H. *ACS Omega* **2017**, *2*, 2577–2582.
- (33) Khalavka, Y.; Ohm, C.; Sun, L.; Banhart, F.; Sönnichsen, C. *J. Phys. Chem. C* **2007**, *111*, 12886–12889.
- (34) Kujala, S.; Canfield, B. K.; Kauranen, M.; Svirko, Y.; Turunen, J. *Opt. Express* **2008**, *16*, 17196–17208.
- (35) Chen, Y.-S.; Frey, W.; Kim, S.; Homan, K.; Kruizinga, P.; Sokolov, K.; Emelianov, S. *Opt. Express* **2010**, *18*, 8867–8878.
- (36) Bosman, M.; Zhang, L.; Duan, H.; Tan, S. F.; Nijhuis, C. A.; Qiu, C.-W.; Yang, J. K. *Sci. Rep.* **2015**, *4*, 5537.
- (37) Sivis, M.; Duwe, M.; Abel, B.; Ropers, C. *Nat. Phys.* **2013**, *9*, 304–309.
- (38) Mesch, M.; Metzger, B.; Hentschel, M.; Giessen, H. *Nano Lett.* **2016**, *16*, 3155–3159.
- (39) Pan, J.; Pafchek, R. M.; Judd, F. F.; Baxter, J. B. *IEEE Trans. Adv. Packag.* **2006**, *29*, 707–713.
- (40) Baram, M.; Chatain, D.; Kaplan, W. D. *Science* **2011**, *332*, 206–209.
- (41) Ringe, E.; Langille, M. R.; Sohn, K.; Zhang, J.; Huang, J.; Mirkin, C. A.; Van Duyne, R. P.; Marks, L. D. *J. Phys. Chem. Lett.* **2012**, *3*, 1479–1483.
- (42) Allen, M. L.; Aronniemi, M.; Mattila, T.; Alastalo, A.; Ojanperä, K.; Suhonen, M.; Seppä, H. *Nanotechnology* **2008**, *19*, 175201.
- (43) Sundar, A.; Hughes, R.; Farzinpour, P.; Gilroy, K.; Devenyi, G.; Preston, J.; Neretina, S. *Appl. Phys. Lett.* **2012**, *100*, 013111.
- (44) Metzger, B.; Hentschel, M.; Lippitz, M.; Giessen, H. *Opt. Lett.* **2012**, *37*, 4741–4743.
- (45) Lippitz, M.; van Dijk, M. A.; Orrit, M. *Nano Lett.* **2005**, *5*, 799–802.
- (46) Metzger, B.; Steinmann, A.; Giessen, H. *Opt. Express* **2011**, *19*, 24354–24360.